INTERNATIONAL JOURNAL OF ENERGY STUDIES

e-ISSN: 2717-7513 (ONLINE); homepage: https://dergipark.org.tr/en/pub/ijes

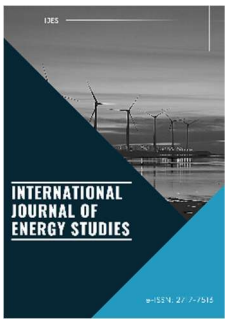

Research Article

Int J Energy Studies 2023; 8(3): 423-451

DOI: 10.58559/ijes.1329160

Received	:	18 July 2023
Revised	:	27 July 2023
Accepted	:	04 Aug 2023

Numerical investigation of PV module cooling process by developing single-pass and doublepass PVT collectors

Erhan Arslan[a*]

[a]*TUBITAK Marmara Research Center, 41470 Gebze, Kocaeli, Türkiye, ORCID: 0000-0002-7540-7935*

*(*Corresponding Author:erhana1985@gmail.com)*

Highlights

- Energy demand of Antarctic reseacrh stations is compared for 16 locations
- Optimum renewable system is calculated for each location
- Maximum renewable factor is obtained for all locations

You can cite this article as: Arslan E. Numerical investigation of PV module cooling process by developing single-pass and doublepass PVT collectors. Int J Energy Studies 2023; 8(3): 423-451.

ABSTRACT

In this study, single-pass and double-pass photovoltaic thermal collectors were designed and analyzed numerically. Energy efficiency and heat transfer coefficients of the PV module were calculated in the study. For case studies two different meteorological conditions (winter and summer) choosed. Case studies were performed with three different Reynolds number (15059, 17805, 22061). Avarage thermal efficiencies obtained for single and double-pass PV-T calculated in winter 65.15% and 67.88% ; summer 56.09%, and 58.46% conditions, respectively. For double- as PV-T, these values are It has been determined that the temperature of the PV module decreases with the increase in flow rate. Avarage electrical efficiency for single pass PVT in winter condition determined as 13.68% where for summer it was calculated as 13.24%. For double pass PVT these values obtained as 14.40% and 13.94%, respectively.

Keywords: Photovoltaic thermal collector, PV cooling, Energy efficiency, CFD

1. INTRODUCTION

Photovoltaic-thermal systems can produce thermal and electrical efficiency simultaneously. For more efficient PV-T systems, the PV module is cooled. These cooling processes have advantages and disadvantages compared to each other.For the optimization of PV cooling performance, the most appropriate parameter (flow rate, solar radiation, etc.) should be determined. . Companies (SolVar Systems and Meyer Burger company) reported that they produce PVT systems with electrical and thermal efficiencies of 15-17.4% and 50-60%, respectively. [1]. Tonui et al. (2007), in their experimental and numerical study, chose air as the working fluid to cool the glassed and non-glass PV-T system. Experimental results are given in comparison with numerical results. The results of the PV-T collector designed as natural circulation have matched each other experimentally and numerically. It was concluded that adding fins to the system provides an improvement in PV efficiency [2]. Cuce et al. (2013) used statistical data in his comprehensive study to determine how the voltage-current characteristics in the PV cell affect the system performance. Experiments using two types of PV models (polycrystalline and monocrystalline silicon PV module) were carried out in an environment with 200-500 W/m^2 solar radiation and a temperature of 15-60°C. Experimental results showed that solar radiation intensity affects current and PV cell temperature affects voltage parameters [3]. Huang, et al. (2001) determined by their experimental study that 20% of the incoming solar radiation of PV cells was given to electricity and the remaining 80% to the environment as waste heat [4]. Amori et al. (2014) carried out the cooling process by placing a fan motor under the panel in their study to numerically examine the cooling of the PV panel with MATLAB simulation. They designed and compared four different PV-Ts using air as the working fluid. Model 1: control panel, model 2: single-channel double-pass, model 3: double-channel single-pass and model 4: single-channel single-pass PV-T's designed as model 3 with the highest average efficiency, followed by model 2 and model 4 determined. It has been determined that the single channel single-pass has the highest electrical efficiency. In addition, it has been stated that the power consumed for cooling the PV module increases in proportion to the flow rate and the model with the least power consumption is model 3. It is said that there is an optimum mass flow rate for each model, and it is concluded that the electrical efficiency increases with the increase of the flow rate [1]. Ceylan and Gürel (2015) experimentally examined the cooling of the PV module in their study. The PV efficiency of the system was 17% at 45°C and the exergy efficiency was 21% at 55°C [5]. Saloux and Teyssedou (2013), in their study, tested the efficiency of PV module and PV-T module with exergy method in 500 W/m^2 and 18°C ambient conditions, and exergy losses were calculated for each system. As a result of the

experiments, it was emphasized that the PV efficiency is strongly dependent on the outdoor temperature and it was observed that the module in PV-T has higher energy and exergy efficiency than normal PV. In addition, it has been determined that the best yield among PV yields in monocrystalline, polycrystalline and amorphous silicon material structure belongs to monocrystal [6]. Infield et al. (2000) examined the effect of flow on efficiency in a study in which they evaluated the performance of double-glazed PVs cooled with air by mounting them on the facade. They found that the efficiency was 25.8% when the flow rate was 0.3 m/s [7]. H.P. Garg and R.S. Adhikari numerically analyzed the performance of the air-cooled PV-Tcollector with the help of simulation. In their study, they investigated how the use of single and double glass in PV-Taffects the performance. As a result, they found that the use of single and double glass affects thermal efficiency depending on the ambient temperature conditions [8, 9]. Bosonac et al. (2003) examined the analysis of air-cooled PV-T that can be integrated into the building. In the study, which was carried out considering the Danish climatic conditions, firstly, studies were made for the optimum flow rate and the design was made to pass 40-50 m^3 air per square meter. In this case, the total efficiency of the system was determined to be 45-47%. PV cells worked at maximum efficiency due to the low outdoor temperature [10]. Tiwari and Sodha (2006) examined the performance analysis of 4 different types of experimental air-cooled PV-T collectors. Glazed and unglazed glass PV-T's are designed with and without tedlar. The use of tedlar in unglazed models showed a decrease in PV cell temperatures. However, there was a slight decrease in the temperature of the outlet air in PV-T, which is not used in glazed models. In addition, it was stated that the increase in the length of the panel reduced the total efficiency, and they found that this was due to the proportional increase in losses as the length increased. PV cell efficiency increased with decreasing cell temperatures [11].

Table 1 shows the some study in literatüre. According to Table 1, as mass flow rate increasing the electrical efficiency of the PV-T is increasing. Also, PV-T systems with channel more efficienct than without channel.

Table 1. Numerical and experimental studies available in the literature

Study	PV type / working fluid / PV-T shape	Electrical Eff.	Thermal Eff.	Total Eff.	Place / Time	Study remarks
[12]	Monocrystalline PV, air type cooling, aluminium-square-rectangle shape cahannel	%11	%51	%62	Hong Kong, 08:00-18:00	Experimental study were done in different weather condition
[13]	Monocrystalline PV, water type cooling-BIPV-T system.	%14.2 %14.6 %13.8 %14.5	%40.2 %65 %78 %40	%54 %80 %91 %55	New Zealand 08:00-18:00	Aspect ratio is 1.5;
[1]	Polycrystalline PV, air type cooling, PV-T module	%9.4	%46	%55	Iraq 06:00-17:00	Double-pass, one channel PV-T with 0.0991 kg/s mass flow rate and environmental condition is 44.3°C
[14]	Polycrystalline PV, water type cooling, BIPV-T,system	%10.8	%48	%59	Malaysia 10:00-17:00	The condition determined as 0.027 kg/s, 690 W/m^2 'solar radiation.
[15]	Monocrystalline PV, air type coolig BIPV-T system	%13.11	%30	%43	Delhi	Channel system produced 9.8% more electrical energy than without channel.
[16]	Monocrystalline PV, air type cooling	%10.5	%50	%61	Italy	Air is used as the working fluid in numerical study.
[17]	Monocrystalline PV, air type cooling	%12	%71.5	%84	Norway	A simulation study of PV / T systems was conducted for a Norwegian residential building trying to achieve a net zero energy balance.

However, PV-T systems, where air is used as the working fluid, are more preferred for cooling the PV module, as the water may freeze in winter conditions [18]. In addition, the research on air PV-T systems with easy manufacture, low cost and low operating expense has been studied extensively. The resulting hot air for space heating, product drying, etc. can be installed [19].

It is possible to come across studies in which the energy analysis of PV-T is performed frequently, when the literature studies are examined. However, studies examining the heat transfer coefficient from the PV-T surface are limited and, it is very rare to encounter studies for double-pass PV-T. In this study, in addition to examining the heat transfer coefficient from the PV-T surface, a double-pass PV-T was designed and analyzed numerically. The validaiton of study were examined by an experimental study [20] in literature and boundary conditions were the same with experimental value. The heat transfer was tried to be increased by integrating the absorber plate into the PV-T collector. In addition, fins were attached to the absorber plate and its effect on efficiency was examined. It is aimed to cool the PV module in numerical study in which air is used as the working fluid. The effect of cooling on electrical efficiency has been examined, the electrical and thermal efficiencies of single-pass and double-pass PV-Ts have been calculated, and their superiority over each other has been discussed.

2. MATERIALS AND METHOD

2.1. Defining Case Studies

In the table below, the names of the case studies in the numeric studies and the boundary conditions are given. These boundary conditions taken an experimental study [20]. Accordingly, Case.a_1, Case.d_1, Case.a_2 and Case.d_2 at a flow rate of 0.11 kg/s; Case.b_1, Case.e_1, Case.b_2 and Case.e_2 0.013 kg/s flow rate and Case.c_1, Case.f_1, Case.c_2 and Case.f_2 0.015 kg/s flow rate. In case studies prepared in accordance with the experimental study, studies were prepared in different boundary conditions as the application of winter and summer conditions. Accordingly, solar radiation values of 900 W/m^2 and 1100 W/m^2 are defined as the boundary condition, respectively. The temperatures included in the experimental study as the inlet air to the collector are defined as boundary conditions. Accordingly, in case studies prepared for winter conditions, the inlet air temperature was defined as 15°C and 24°C degrees for winter and summer applications, respectively (Table 2).

Table 2. Description of the case studies

		Winter				Summer		
Collector type	**Reynolds number**	**Inlet temperature (°C)**	**Solar Radiation W/m²**	**Name of the case studies**	**Reynolds number**	**Inlet temperature (°C)**	**Solar Radiation W/m²**	**Name of the case studies**
Single-pass	15059	14,20		Case. a_1	14662	24,20		Case. a_2
	17805	13,84		Case. b_1	17351	23,54		Case. b_2
			900				1100	
	22061	15,30		Case. c_1	20069	23,09		Case. c_2
Double-pass	15059	14,20		Case. d_1		24,20		Case. d_2
	17805	13,84		Case. e_1		23,54		Case. e_2
	22061	15,30		Case. f_1		23,09		Case. f_2

2.1. Energy Analysis

In photovoltaic systems, heat and electrical energy is obtained when solar radiation reaches the absorber surface. In a PV-Tmodule, the electrical efficiency is much lower than its thermal efficiency and hence the overall efficiency will depend largely on the thermal energy of the protection. Overall energy efficiency ignores the difference between heat and electrical energy in terms of energy class and is therefore insufficient to fully verify energy performance in PV-T systems [21] Table 3 contains the components of the PV-T collector designed for this study and the thermophysical properties of these materials.

Table 3. Measurements and thermophysical properties of the system components

Systme component	**Parameter**	**Symbol**	**Value**	**unit**
PV-T Collector	Area	A_{pvt}	0.65	m^2
	Lenght	L	1.1	m
	Width	W	0.5	m
	Depth	δ	0.09	m
PV Module	Thickness	δ_{pv}	0.0003	m
	Specific heat	$c_{p_{pv}}$	677	J/kgK
	Density	ρ_{pv}	2330	kg/m^3
	Emissivity	ε_{pv}	0.88	-
	Absorptivity	α_{pv}	0.95	-
	Thermal conductivity	k_{pv}	148	W/mK
	Transmisivite	τ_{pv}	0.88	-
	Reference cell efficiency	η_{ref}	0.12	-
Fin Structure	Thickness	δ_{plate}	0.001	m
	Spesific heat	$c_{p_{plate}}$	381	J/kgK
	Density	ρ_{plate}	8978	kg/m^3
	Emissivity	ε_{plate}		-
	Absorbsivity	α_{plate}		-
	Thermal conductivity	k_{plate}	388	W/mK
Insulation Material	Thickness	δ_{ins}	0.02	m
	Spesific heat	$c_{p_{ins}}$	880	J/kgK
	Density	ρ_{ins}	15	kg/m^3
	Emissivity	ε_{ins}	0.05	-
	Absorbsivity	α_{ins}		-
	Thermal conductivity	k_{ins}	0.041	W/mK

The efficiency of the solar cell as a function of temperature or the efficiency of the solar cell depending on the temperature are calculated with the help of Eq. (1). The expression of the electricity produced by the solar radiation coming to the PV panel in terms of efficiency is given in Eq. (1) [22].

$$\eta_{pv} = \eta_{ref}\left[(1 - \beta\left(\mathrm{T}_{pv} - \mathrm{T}_{ref}\right)\right] \quad (1)$$

Current-voltage values produced by the PV panel are among the values measured in the thesis study. Electrical efficiency expression as function of current-voltage It is given in Eq. (2) [23]:

$$\eta_{el} = \frac{P_{max}}{AxG},\ P_{max} = IxV \quad (2)$$

Here η_{ref} is the standart test condition electrical efficiency 1000 $\frac{W}{m^2}$ and is taken as 0.12. $\beta_0 = \frac{1}{T_{film}}$ and $T_{film} = \frac{\mathrm{T}_{pv}+\mathrm{T}_{ref}}{2}$ (K), T_{ref} means the reference cell temperature and was taken as 25°C. Thermal efficiency and total efficiency of the PV-T collector are given Eq. (3) and Eq. (4):

$$\eta_{th} = \frac{Q_u}{AxG},\ Q_u = \dot{m}c_p\,(T_{out} - T_{in}) \quad (3)$$

$$\eta_{PV/T} = \eta_{th} + \eta_{el} \quad (4)$$

The Reynolds number for air flow inside solar air heater could be calculated as Eq. (5):

$$Re = \frac{\rho V\ \ h}{\mu} \quad (5)$$

where the Nusselt number could be expressed by Eq. (6)

$$Nu = \frac{hD_h}{k} \quad (6)$$

Wall heat transfer coefficiecnt given by Eq. (7)

$$h_{wall} = \frac{q}{T_{pv} - T_{fluid}} \quad (7)$$

2.2. Computational Fluid Dynamics Analysis

Computational Fluid Dynamics (CFD) and Numerical analysis are explained mathematically with the help of equations related to momentum, conservation of mass and energy. Partial differential equations (PDDs) define fluid as a continuous medium. These techniques are used to solve the problem by replacing the SEDs with algebraic equations when the physical field is divided into several separate control volumes. Each of the control volumes are called cells or elements. These cells show algebraic relationships on how flow variables such as temperature, velocity, and pressure change in local settings with space coordinates, which is the main idea behind Computational Fluid Dynamics. On the other hand, CFD simulates fluid engineering systems with the help of solvers, analysis methods, networking and numerical parameters as well as mathematical modeling [24]. Since CFD analysis is performed before experimental tests, it allows different experiments to be carried out during the design process.

• Complete numerical solution (spectrum analysis, etc.) is of course difficult to make in systems such as photovoltaic thermal solar collectors with extreme thermo flow conditions and complex geometries. CFD studies are suitable for such situations.

• As a fundamental and important component of quality, the measurement of CFD quality can be measured by finding a detailed solution for complex systems and time-dependent flows using the latest techniques and technologies.

• The application of numerical models solves physical problems with high accuracy and greater reliability and helps to make mathematical improvements in solution diagrams and turbulence models.

• After the latest developments, solving and predicting a fluid dynamics problem is no longer a difficult thing as it does not require very powerful computers. Only a personal computer is sufficient for this purpose.

Navier-Stokes Equations are equations based on the law of conservation of physical properties of fluids. This principle explains how the properties of the fluid change. These properties depend on the incoming and outgoing energy, mass, and momentum. When the law of conservation of mass

(Eq. 8), Momentum (Eq. 9 and Eq. 10) and Energy (Eq. 11) is applied, a continuity equation can be obtained in addition to the energy equation and momentum equation:

The equations developed for a fluid particle flow represent a mathematical expression of the conservation laws of physics. The most general expression of the conservation of mass (Eq. 6) is as follows [25]. The conservation equation of momentum and energy is Eq. (6) - Eq. (7) and Eq. (8).

Continuity Equation

$$\frac{\partial \rho}{\partial t} + \nabla(\rho v) = 0 \tag{8}$$

Eq. (8) represents the conservation of mass or the continuity equation in three dimensions at a point in a time-dependent compressible flow. The first expression ($\partial\rho/\partial t$) in this equation expresses the change in density with time. This expression is zero because the models made in this study are solved independently of time. The second expression ($\nabla(\rho v)$) is the net mass flow occurring along the boundaries of the fluid element, also known as the convective term [26].

Momentum Equation

$$\frac{\partial(\rho u)}{\partial t} + \nabla(\rho u V) = -\frac{\partial p}{\partial x} + \mu\nabla(\nabla u) + \rho g_x \tag{9}$$

$$\frac{\partial(\rho v)}{\partial t} + \nabla(\rho v V) = -\frac{\partial p}{\partial x} + \mu\nabla(\nabla v) + \rho g_y \tag{10}$$

Conservation of Energy Equation

$$\rho c_p \left(\frac{dT}{dt} + \nabla TV\right) = \nabla(\nabla kT) \tag{11}$$

The following assumptions have been applied in the solution of continuity, momentum and energy equations in the heat transfer and air flow model for numerical analysis in the photovoltaic-thermal solar collector: [24].

1. Unpressurized turbulent flow and single phase through the channel.

2. Continuous three-dimensional (3D) fluid flow and heat transfer.
3.Steady state condition (fully developed flow)
4. Thermo-physical properties are constant for both solid absorber plate (copper) and fluid (air).
5. Gravity has been neglected

2.2.1. Standard k-epsilon model

In this study, the standard k-ε turbulence model is used to solve the turbulence model. The standard k- ε turbulence model is the most widely used model. There are many terms in the k-ε equations that are unknown and cannot be measured. For a much more practical approach, it can be applied to a large number of turbulent applications in terms of our best understanding of the processes involved, thus minimizing the unknowns. Standard k- ε is a common and widely used two-equation model. The two transport variables that are solved in this model are k, turbulent kinetic energy and, turbulent propagation. This model has been applied to suggest turbulent length scales in complex flows.

It is assumed that the turbulent viscosity (μt) is proportional to the turbulence velocity and the length scale. These scales are derived from turbulent kinetic energy (k) and propagation rate (ε). Turbulent viscosity expression is as follows (Eq. 12) [27].
$C\mu$, is an experimental constant. In the k-ε turbulence model, k and ε values are needed to calculate the turbulent viscosity (μ_t). These values are obtained from the equations given below [28, 29]. The transport equations used to solve k and ε transport transport variables are as follows (Eq. 13-14): Turbulent kinetic energy k,

$$\mu_t = \rho C_\mu \frac{k^2}{\varepsilon} \tag{12}$$

$$\frac{\partial(\rho k)}{\partial t} + \frac{\partial(\partial k u_i)}{\partial x_i} = \frac{\partial}{\partial x_j}\left[\frac{\mu_t}{\sigma_k}\frac{\partial k}{\partial x_j}\right] + 2\mu_t E_{ij} E_{ij} - \rho\varepsilon \tag{13}$$

$$\frac{\partial(\rho k)}{\partial t} + \frac{\partial}{\partial x_j}(\rho U_j k) = \frac{\partial}{\partial x_j}\left[\left(\mu + \frac{\mu_\tau}{\sigma_k}\right)\frac{\partial k}{\partial x_j}\right] + P - \rho\varepsilon + P_{kb} \tag{14}$$

Turbulent dissipation rate ε in Eq. (15),

$$\frac{\partial(\rho\varepsilon)}{\partial t}+\frac{\partial(\partial\varepsilon u_i)}{\partial x_i}=\frac{\partial}{\partial x_j}\left[\frac{\mu_t}{\sigma_\varepsilon}\frac{\partial\varepsilon}{\partial x_j}\right]+C_{1\varepsilon}\frac{\varepsilon}{k}2\mu_t E_{ij}E_{ij}-C_{2\varepsilon}\rho\frac{\varepsilon^2}{k} \quad (15)$$

Turbulence kinetic energy generation due to mean velocity gradient and viscous forces, experimental constants $C_{\varepsilon 1}$ and $C_{\varepsilon 2}$, and σ_ε, σ_k are Prandtl numbers. The values of the constants required for the solution of my equation are given in Table. 4 [28]:

Table 4. Constants used in the k-ε model [30].

$C_{\varepsilon 1}$	$C_{\varepsilon 2}$	C_μ	σ_ε	σ_k
1.44	1.92	0.09	1.3	1.0

As in many approaches, there are negligence assumptions in this model as well. Consequently, the modeled ε transport model can be used in a form and in a very similar form to the k transport equation.

2.3. Creating the Model, Mesh Structure and Boundary Conditions

ANSYS 18.2 has used Fluent software for thermal simulation and estimation of temperature development at different focal points of the PV-Tcollector. "Design Modeler", a sub-program of ANSYS, has been used to draw the 3-D flow field [31]. "Mesh" structure is of great importance in modeling the flow. First, a rough mesh structure was used to show flow. For the solution of momentum, continuity and energy equations, a finite volume method "second order upwind scheme" was used. "SIMPLE" algorithm was chosen for discretization of basic equations. While an average heat flux condition is applied to the surface of the PV module, an adiabatic boundary condition has been applied to all other surfaces of the PV-T. All other surfaces are considered completely insulated with zero heat flux. "No slip condition" condition has been applied to all surfaces. The inlet air velocity is considered homogeneous and the pressure condition is applied at the outlet. 10E-6 for the "residual" of the continuity equation, 10E-6 for the "residual" of the velocity components and 10E-8 for the "residual" of the energy. After getting the first results, the mesh structure was made thinner in certain places to achieve better results.

Standard k-ε turbulence model has been chosen as the turbulence model. Geometry and mesh structure are shown in Fig. 1 and Fig. 2. Continuity, momentum and energy equations are solved by 10E-6 convergence criteria. A high resolution recommendation scheme has been chosen for

discretization of the terms pressure, velocity and temperature. Spherical dynamic model controls are adapted to solve continuity, momentum and energy equations.

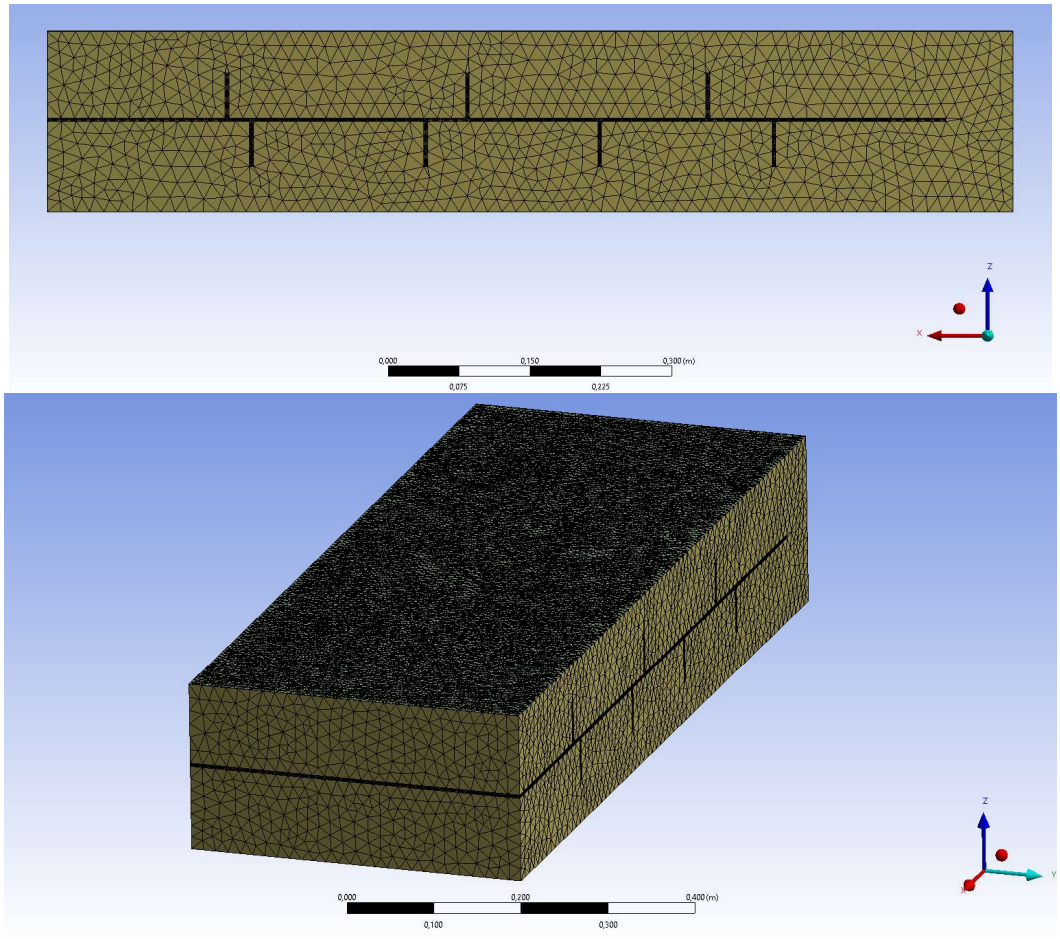

Figure 1. Mesh structure of the geometry up: side view down: front view

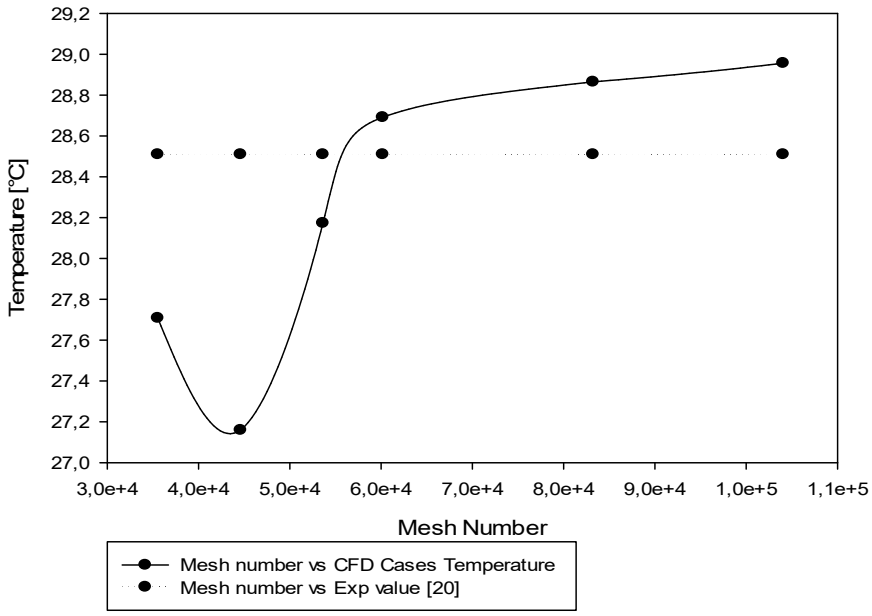

Figure 2. Variation of outlet temperature of solar heaters via mesh element number *

$\dot{m} = 0.11\frac{kg}{s}$ and SPPVT winter condition situtaiton has been considered *

2.4. Geometry Structure

Double-pass PV-T collector were designed for obtaining more electrical power. Cooling by air in double-pass collector, is would be more effective. For having more thermal efficiency, the fins attached to the collector. In Fig. 3 and Fig. 4 has shown the new type designed PV-T collector. Fig.3 and Fig. 4 shows the geometries of SP and DP, respectively. Fins are attached to the absorber plate to increase the heat transfer surface. In the numerical study, it consists of two domanines: air (fluid), absorber plat and fins (solid).

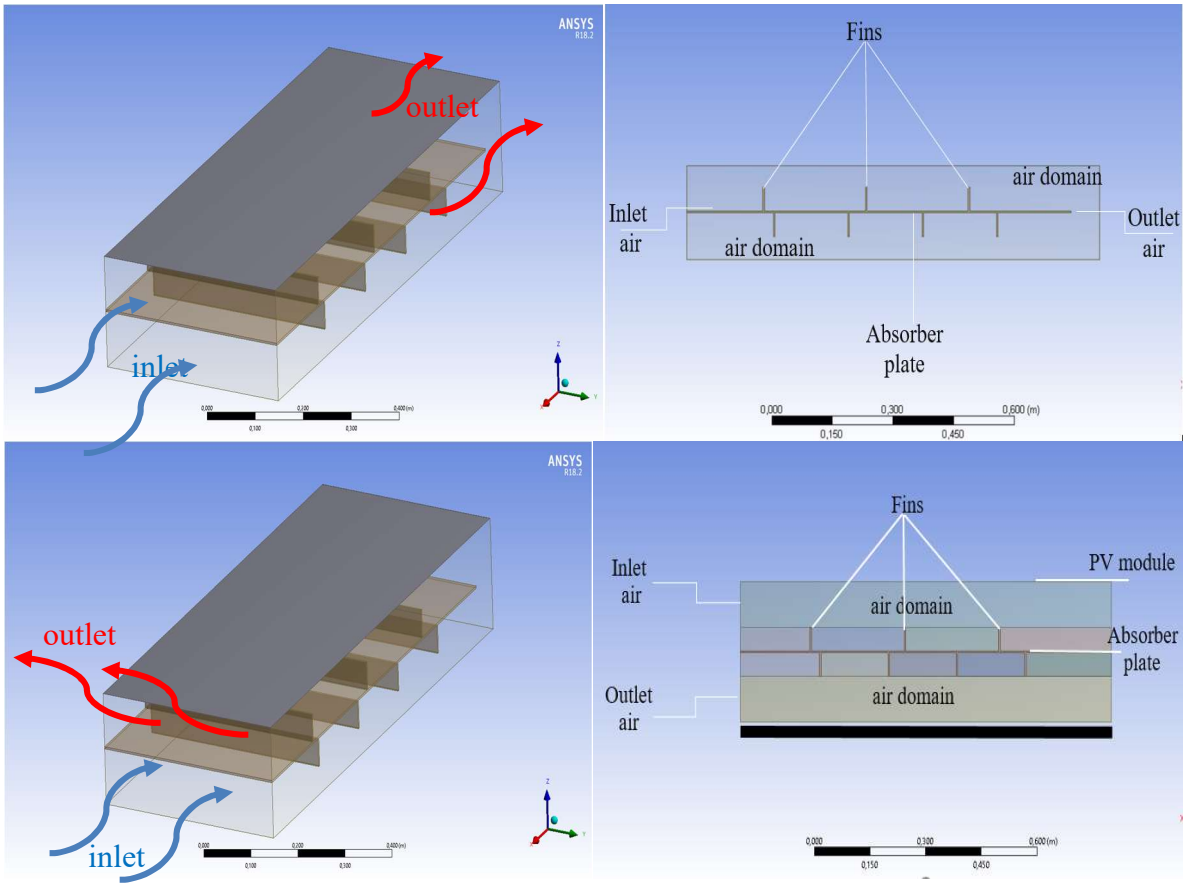

Figure 4. Geometry of the double-pass PV-T collector with system components

3. RESULTS

The results obtained as a result of the analysis are shown below. Accordingly, it was observed that the PV surface temperature decreased with the increase of the flow rate. Electrical efficiency increases as the PV surface temperature decreases. Fig. 5 (a) and Fig. 5(b) show the location of three lines, which are the measurement points of the SP and DP collectors, respectively. In order to calculate the temperature and heat convection coefficient, measurements were taken from different sections (Line 1, line 2 and line 3). Thus, it was aimed to examine how the temperature distribution on the PV surface is affected by the flow and the effects on heat convection.

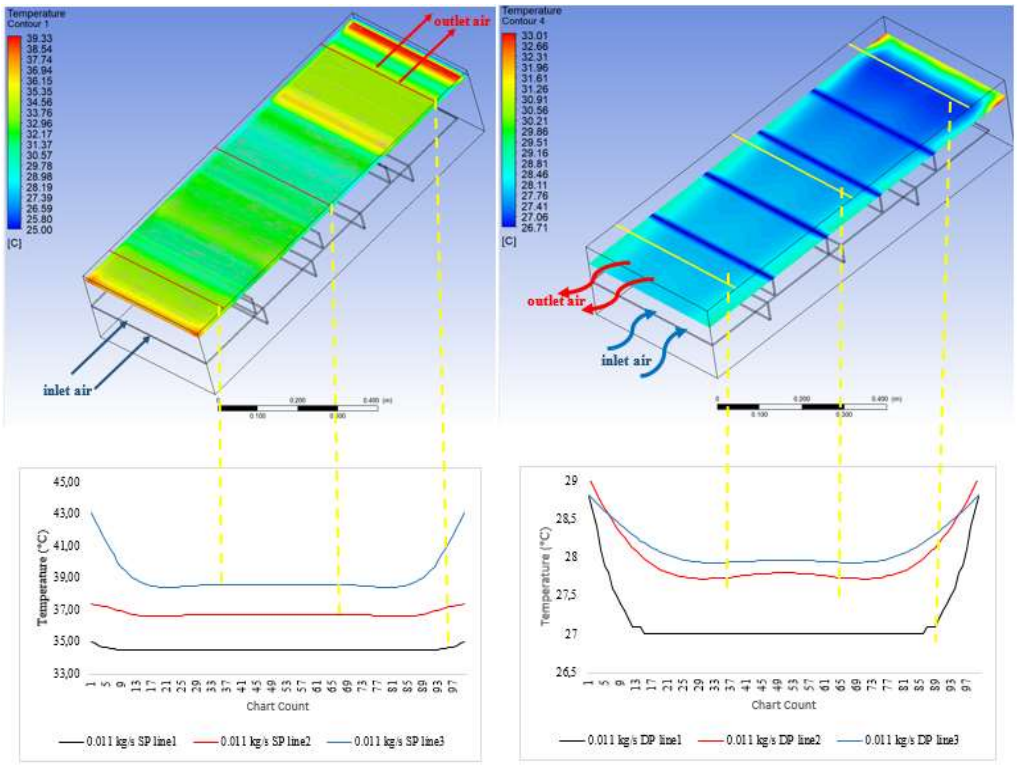

Figure 5. Representation of the measured points in geometry on the line 1, line 2, line 3 (a) SinglepassPV-T (SPPVT) b) Double-pass PV-T (DPPVT)

Fig. 6 shows the variation of heat transfer coefficient by chart count under winter condition (*inlet Temperature: 15°C, and solar radiation: 900 W/m^{2}K*) for SPPVT. Accordingly, the average heat transfer coefficient values for Line1, Line2 and Line 3 for Case.a_1 were measured as 0.58 W/m^{2}K, 3.44 W/m^{2}K and 3.68 W/m^{2}K. For Case.b_1, these values were obtained as 0.70 W/m^{2}K, 3.99 W/m^{2}K and 4.23 W/m^{2}K, respectively. For Case.c_1, it was determined as 0.84 W/m^{2}K, 4.56 W/m^{2}K and 4.78 W/m^{2}K, respectively.

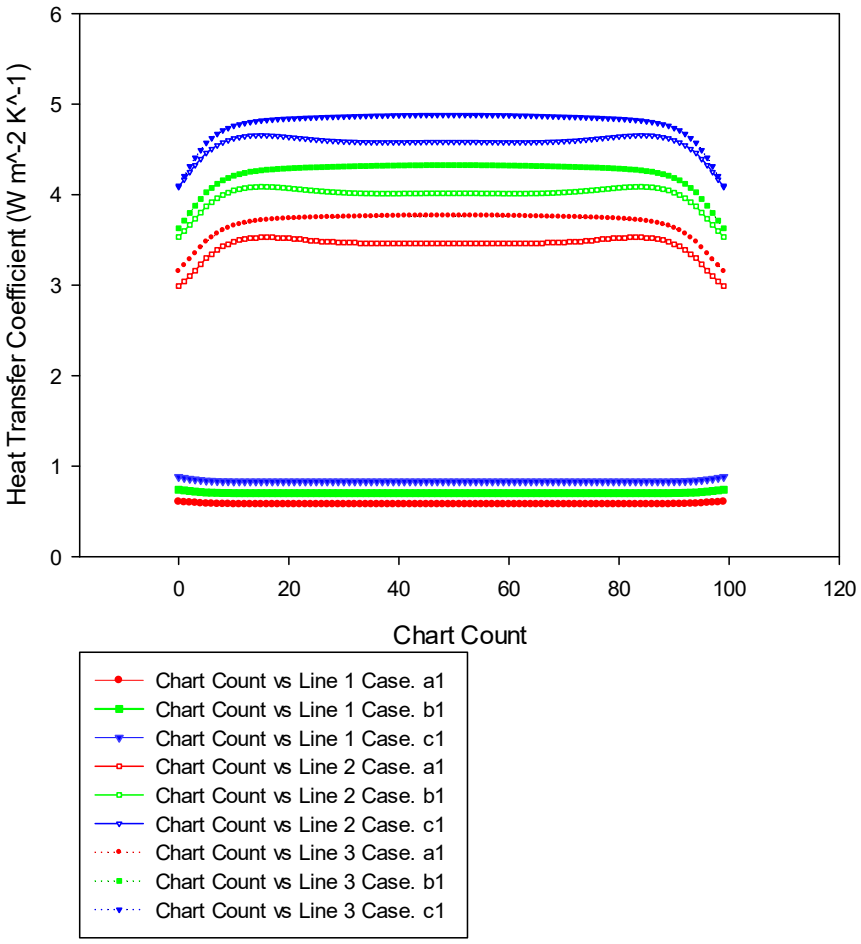

Figure 6. Variation of the heat transfer coefficient for SPPVT under winter condition

Fig. 7 shows the change of heat transfer coefficients taken in winter applicacitons for DPPVT taken over Line 1, Line 2 and Line 3 in the Case. d_1 study is given below. Accordingly, the average values of the heat transfer coefficients were obtained as 6.07 W/m^{2}K, 6.89 W/m^{2}K and 1.40 W/m^{2}K, respectively. For Case. e_1, these values were found to be 6.98 W/m^{2}K, 7.84 W/m^{2}K and 1.74 W/m^{2}K. It was calculated as 7.85 W/m^{2}K, 8.73 W/m^{2}K and 2.13 W/m^{2}K for Case. f_1.

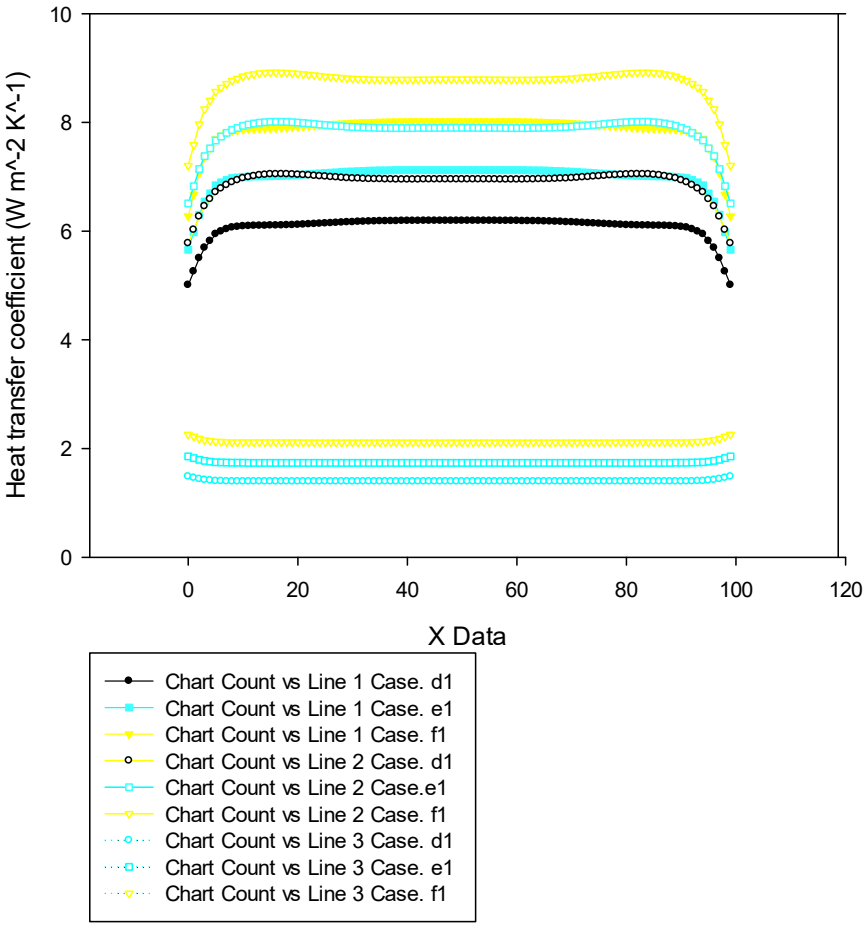

Figure 7. Variation of the heat transfer coefficient for DPPVT under winter condition

Fig. 8 shows the change temperature by chart count in winter applications for SPPVT. Temperature values taken from Line 1, Line 2 and Line 3 for Case.a_1 is given below. Accordingly, the average values of the temperature values taken over the Lines were obtained as Case. a_1 49.10°C, 55.22°C and 64.12°C, respectively. For Case.b_1, these values were determined as 46.03°C, 51.40°C and 58.42°C, respectively. For Case.c_1, these values were determined as 43.58°C, 48.55°C and 54.12°C, respectively.

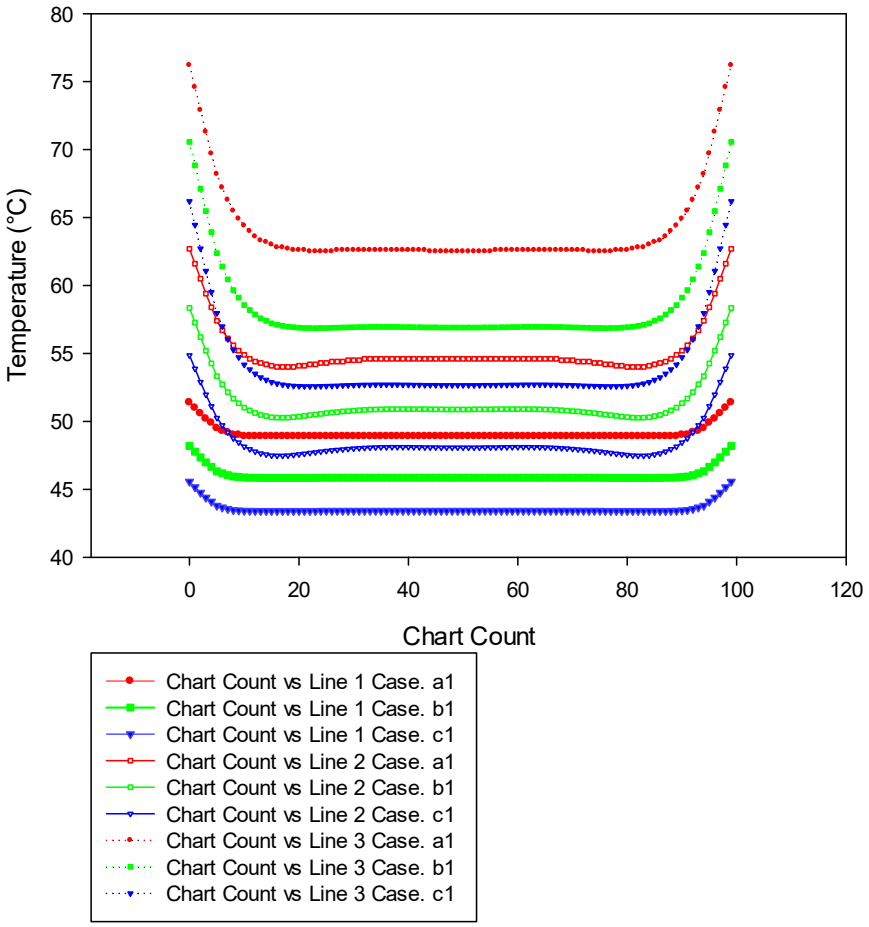

Figure 8. Variation of the temperature for SPPVT under winter condition

Fig. 9 shows the temperature values of taken from Line 1, Line 2 and Line 3 in Summer applications for SPPVT. Accordingly, the average temperature values were determined as for Case.a_2 59.10°C, 65.23°C and 74.12°C, respectively. For Case.b_2, these values were determined as 55.03°C, 60.41°C and 67.43°C, respectively. Mean temperature values for Case.c_2 were obtained as 53.58°C, 58.55°C and 64.12°C, respectively.

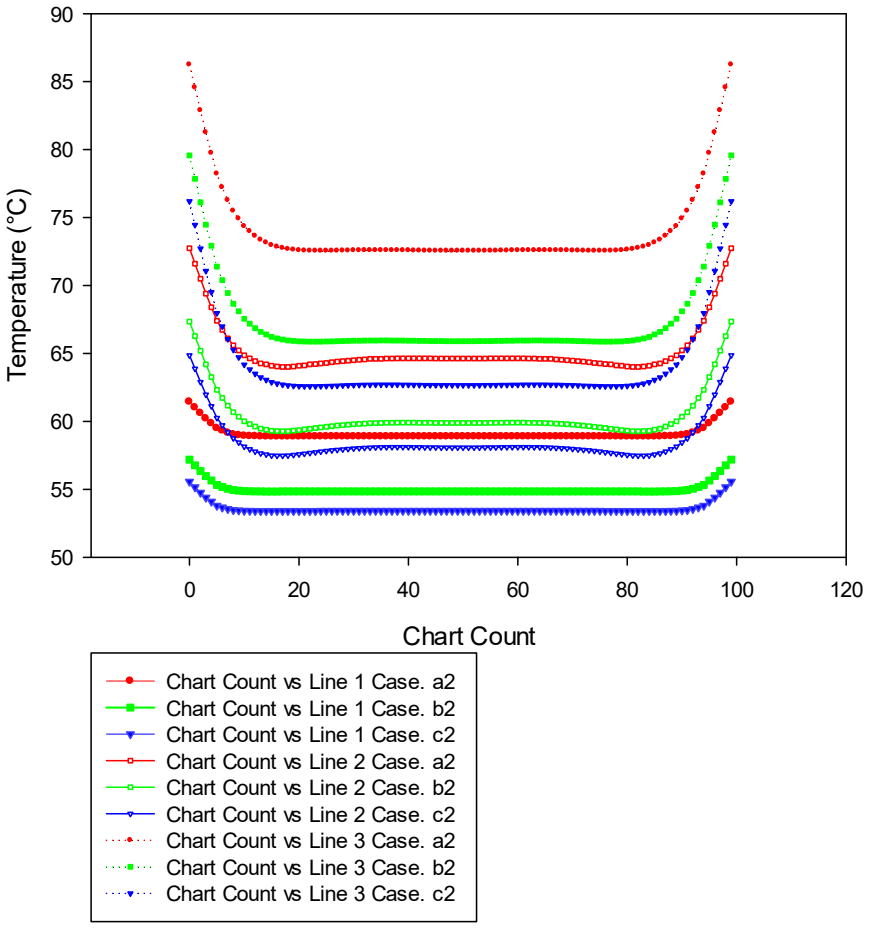

Figure 9. Variation of the temperature for SPPVT under summer condition

The graph of the temperature values taken from Line 1, Line 2 and Line 3 for winter applications of the DPPVT given in Fig. 10. Accordingly, the average values of the temperature values taken over the Lines were obtained as for Case.d_1 46.46°C, 37.94°C and 33.30°C, respectively. For Case.e_1, these values were determined as 42.76°C, 35.75°C and 31.35°C, respectively. For Case.f_1, these values were determined as 39.81°C, 33.94°C and 29.77°C, respectively.

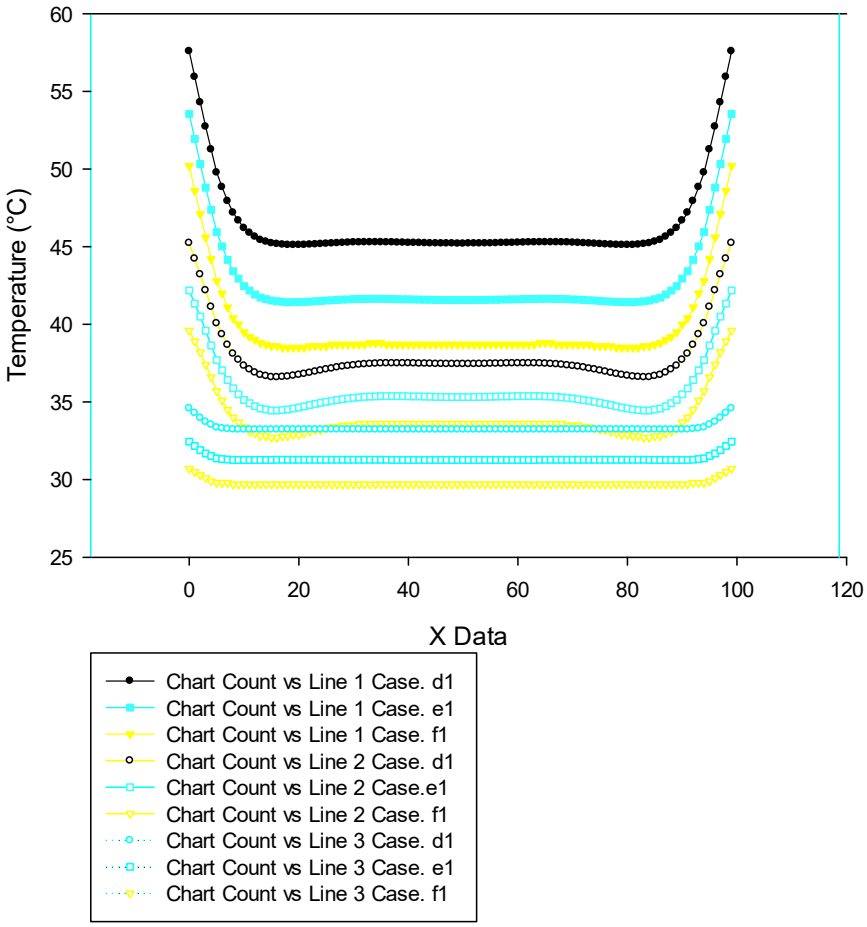

Figure 10. Variation of the temperature for DPPVT under winter condition

Fig. 11 shows the variation of temperature by chart count. Values taken from Line 1, Line 2 and Line 3 for Case.d_2 is obtained as 56.46°C, 47.94°C and 43.29°C, respectively. For Case.e_2, these values were determined as 51.75°C, 44.75°C and 40.37°C; for Case.c_2, were determined as 49.81°C, 43.94°C and 39.77°C, respectively.

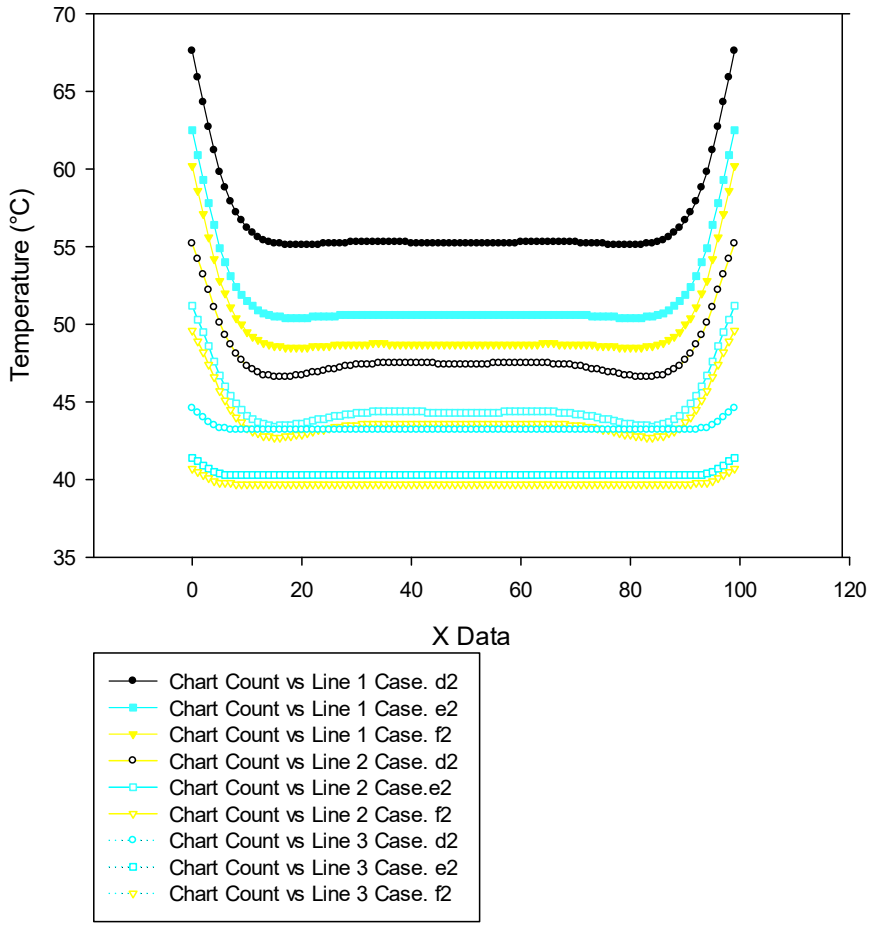

Figure 11. Variation of the temperature for DPPVT under summer condition

The distribution of the PV surface temperature is shown in Fig. 12 and Fig. 13. Accordingly Case. a_1, Case. b_1, Case.c_2, Case. a_2, Case. b_2 and Case. c_2 was determined as 56.43°C, 52.25°C, 49.06°C, 66.43°C, 61.25°C, 59.06°C, respectively (Fig.12). Case. d_1, Case. e_1, Case. f_1, Case. d_2, Case. e_2, Case .f_2 was determined as 39.55°C, 36.91°C, 34.80°C, 49.56°C, 45.91°C, 44.80°C (Fig.13). In all applications, a decrease was observed in the PV surface temperature due to the increase in flow rate. It has been observed that DPPVT's PV surface temperatures are lower than SPPVT in winter applications. Similarly, DPPVT has been observed to have lower PV surface temperature in summer applications.

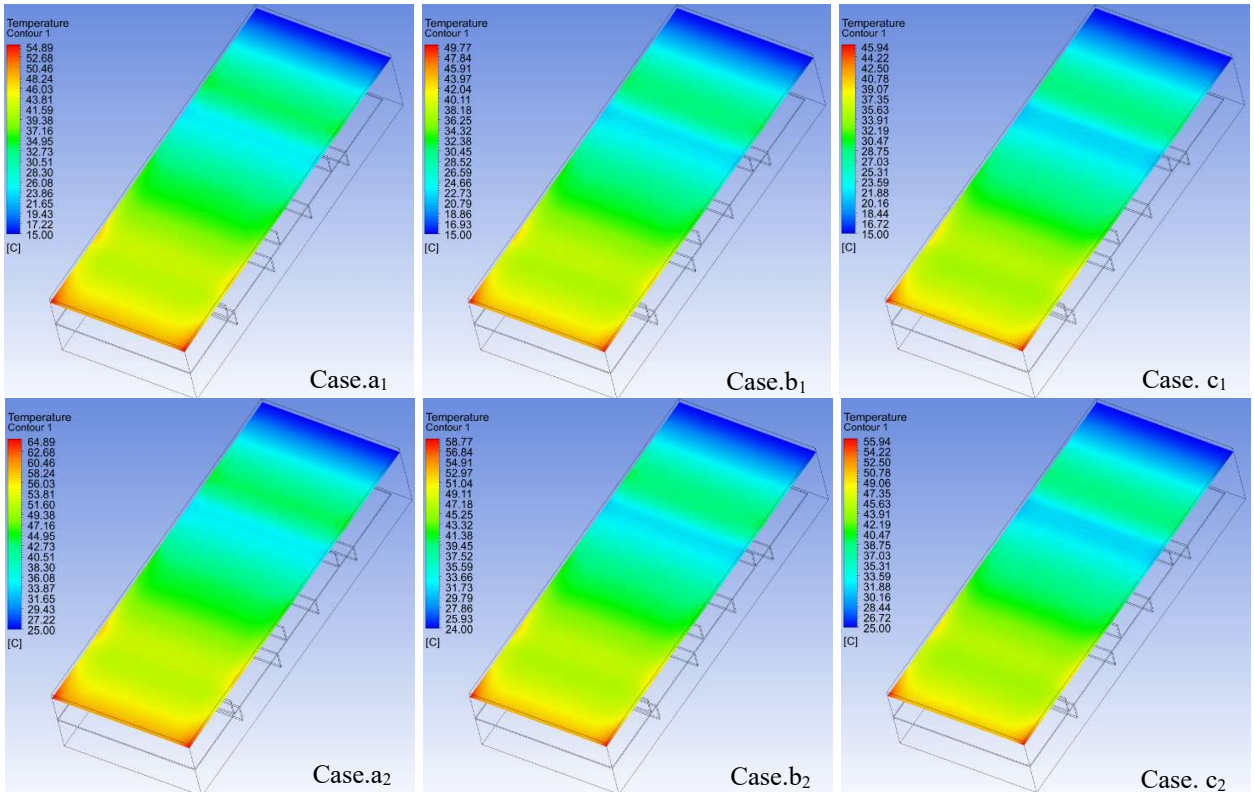

Figure 12. Variation of PV surface temperature for SPPVT for all cases

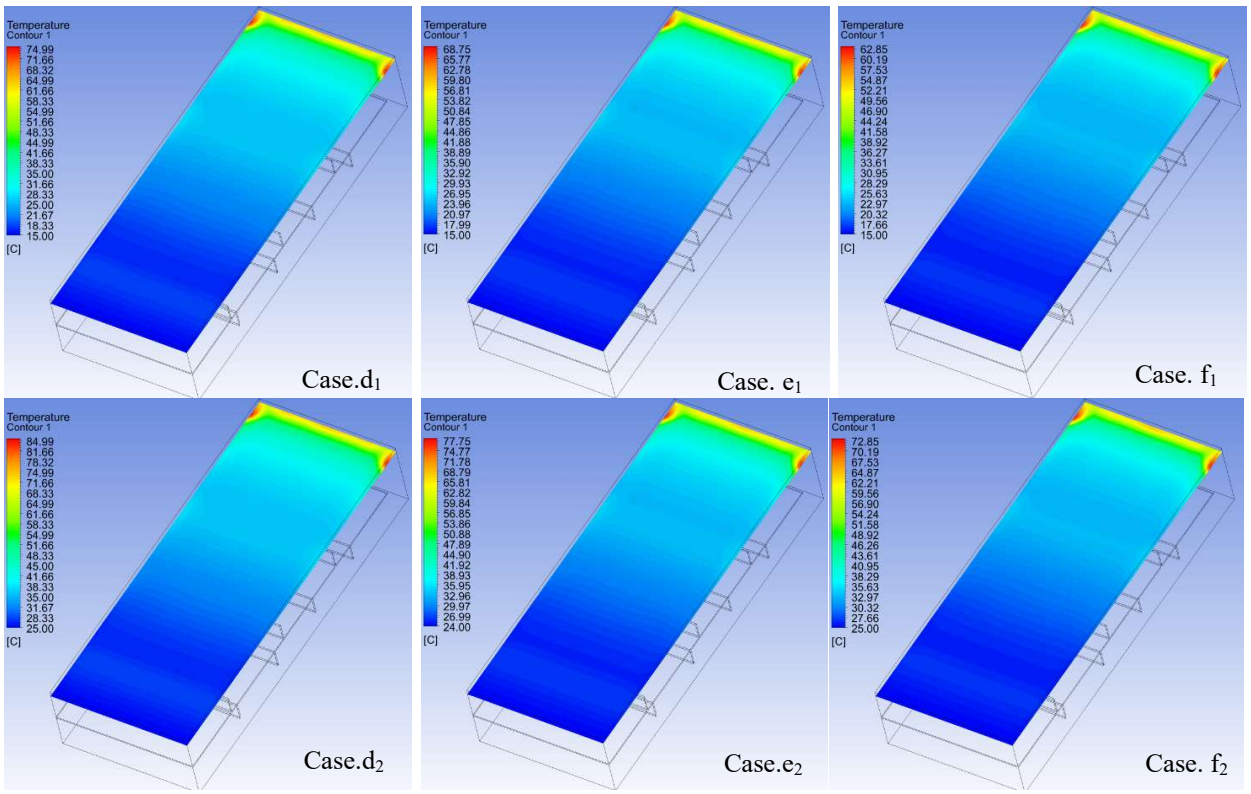

Figure 13. Variation of PV surface temperature for DPPVT for all cases

In the graphs below, the graph of thermal efficiency versus mass flow is given. Accordingly, for Case. a_1, Case. b_1 and Case. c_1, in winter conditions thermal efficiencies obtained as 62.63%, 65.25% and 67.58%, respectively. For the same case studies, the values obtained in the summer application were obtained as 50.84%, 59.03% and 64.91%, respectively (Fig. 14). For Case. d1, Case. e1 and Case. f1, thermal efficiencies obtained as 68.24%, 70.96% and 73.44% in winter conditions; In summer practice, these values were obtained as 54.15%, 62.56% and 60.09% (Fig. 15). Comparison of thermal efficiencies with experimental study is also given in the graphs. Accordingly, it is seen that the thermal efficiencies obtained from case studies are higher.

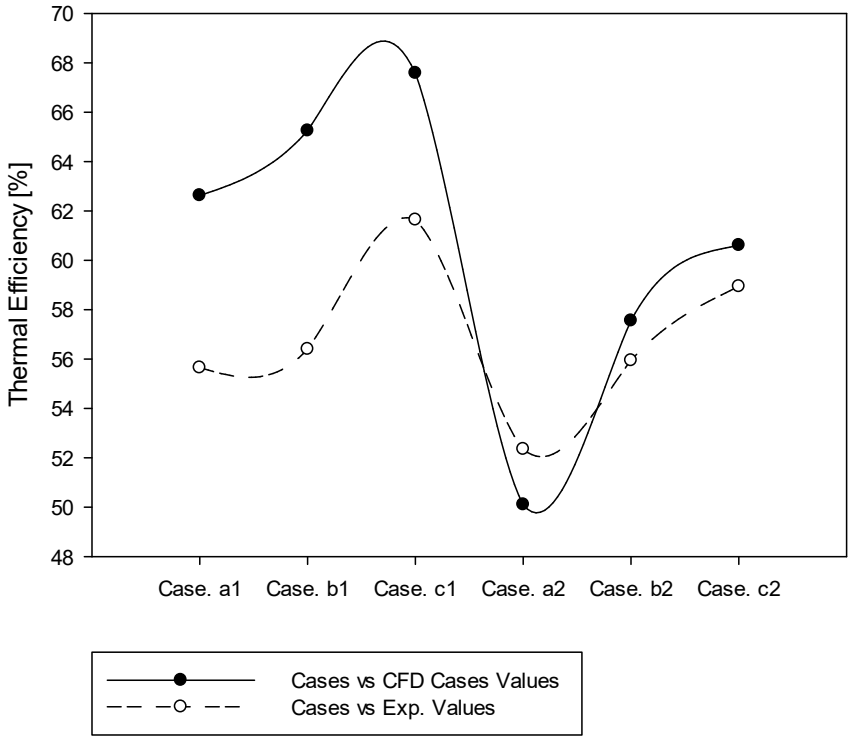

Figure 14. Variation of thermal efficiencies of SPPVT for winter and summer cases for SP

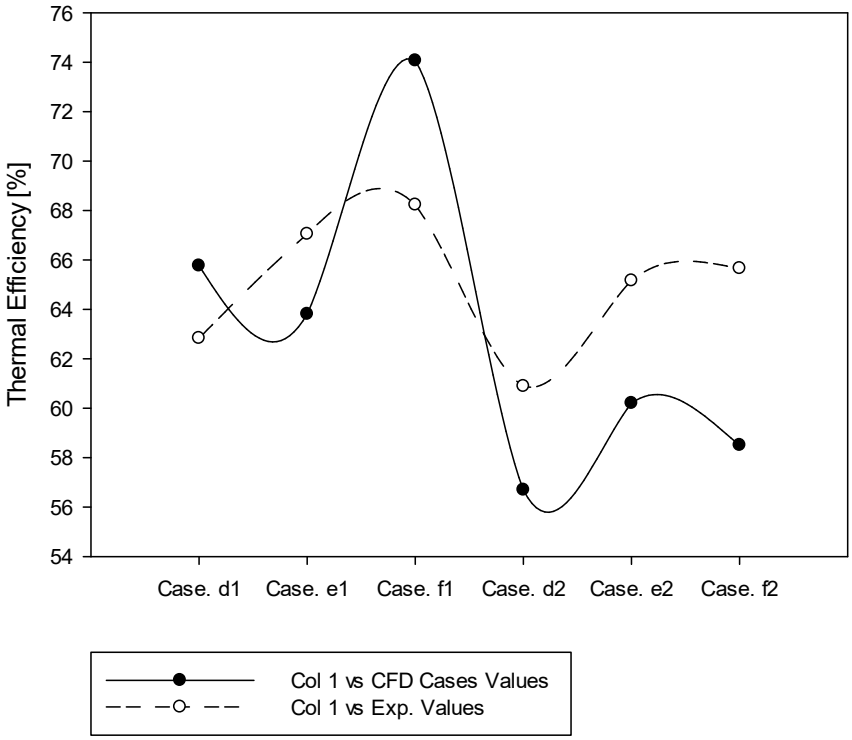

Figure 15. Variation of thermal efficiencies of DPPVT for winter and summer cases

In Fig. 16, comparative electrical efficiencies were determined as 13.50%, 13.69%, 13.84%, 13.05%, 13.28%, 13.38% for SPPVT, respectively, while for DPPVT it was calculated as 14.29%, 14.41%, 14.51%, 13.81%, 13.98%, 14.04% (Fig. 17). It is seen that the results obtained are consistent with previous studies in the literatüre [32-34].

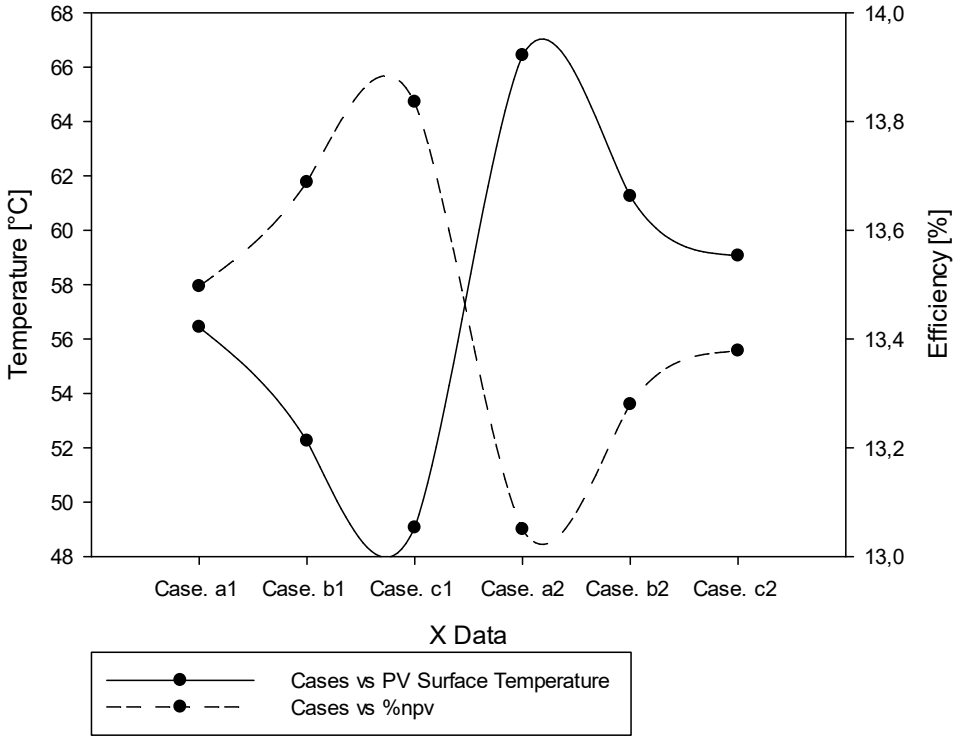

Figure 16. Variation of electrical efficiencies of SPPVT for winter and summer cases with comparation of PV surface temperature

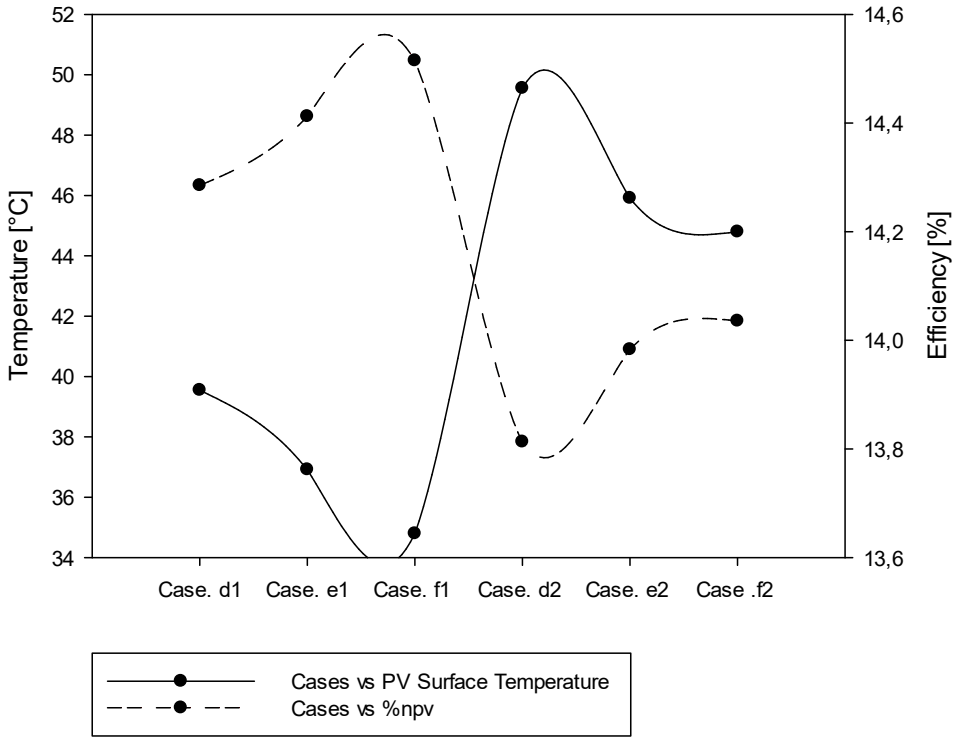

Figure 17. Variation of electrical efficiencies of DPPVT for winter and summer cases with comparation of PV surface temperature

It was concluded that there was an improvement in thermal and electrical efficiency with the increase of efficiency for both collectors. In all experiments, it was determined that the heat transfer coefficient increased with the increase of the flow rate, and it was found that there was an increase in thermal efficiency (due to the increase in the heat transfer coefficient. As a result of the cooling in the PV module, an increase in electrical efficiency was observed.

4. CONCLUSION

In this study, numerical analysis of PV-T collectors has been made. The numerically obtained results were compared with the experimental study and it was found that they were compatible with each other. The superiority of single pass and double pass PV-Ts to each other was investigated. Surface temperatures, heat transfer coefficients, electrical efficiencies and thermal efficiencies at different flow rates (0.011 kg/s, 0.013 kg/s and 0.015 kg/s) were calculated and the following results were obtained:

While the lowest PV surface temperature for SPPVT in winter conditions was determined as Case. c_1 (49.06°C); It was observed in Case. c_2 (59.06°C) in summer conditions. The highest electrical efficiency was calculated as 13.84% and 13.38% for Case. c_1 and Case. c_2, respectively. Thanks to the cooling of the PV surface, an increase of 3.20% in electrical efficiency compared to the average of winter and summer applications has been calculated.

While the lowest PV surface temperature for DPPVT in winter conditions was determined as Case. f_1 (34.80°C); In summer conditions, it was observed that this situation was in Case. f_2 (44.80°C). The highest electrical efficiency was calculated as 14.51% and 14.04% for Case. f_1 and Case. f_2, respectively. Thanks to the cooling of the PV surface, an increase of 3.19% in electrical efficiency compared to the average of winter and summer applications is calculated.

It was observed that electrical efficiency improved by 5.07% and 5.08%, respectively, thanks to the use of double-pass in winter and summer applications.

The highest and lowest thermal efficiencies were found in Case. f_1 and Case. a_2 studies, respectively. Thermal efficiencies were calculated as 74.06% and 50.10%, respectively. There was a 4.01% improvement in thermal efficiency thanks to the use of double pass in winter conditions; On the other hand, this rate was found to be 4.07% in summer conditions.

ACKNOWLEDGMENT

This research did not receive any specific grant from funding agencies in public or not-for-profit sectors.

DECLARATION OF ETHICAL STANDARDS

The author of this article declares that the materials and methods used in this study do not require ethical committee permission and/or legal-special permission.

CONTRIBUTION OF THE AUTHORS

Erhan Arslan: Analyzed the results of the numerical results and wrote the manuscript.

CONFLICTS OF INTEREST

No conflict of interest was declared by the author.

REFERENCES

[1] Amori KE, Abd-AlRaheem MA. Field study of various air based photovoltaic/thermal hybrid solar collectors. Renewable Energy 2014; 63: 402-414.

[2] Tonui J, Tripanagnostopoulos Y. Air cooled PV/T solar collectors with low cost performance improvements. Solar energy 2007; 81(4): 498-511.

[3] Cuce E, Cuce PM, Bali T. An experimental analysis of illumination intensity and temperature dependency of photovoltaic cell parameters. Applied Energy 2013; 111: 374-382.

[4] Huang BJ. Performance evaluation of solar photovoltaic/thermal systems. Solar Energy 2001; 70(5): 443-448.

[5] Ceylan İ, Gurel AE. Exergetic analysis of a new design photovoltaic and thermal (PV/T) System. Environmental Progress & Sustainable Energy 2015; 34(4): 1249-1253.

[6] Saloux E, Teyssedou A, Sorin M. Analysis of photovoltaic and photovoltaic/thermal (PV/T) systems using the exergy method. Energy and Buildings 2013; 67: 275-285.

[7] Infield D, Mei L, Eicker U. Thermal performance estimation for ventilated PV facades. Solar Energy 2004; 76(1-3): 93-98.

[8] Garg HP, Adhikari RS. Conventional hybrid photovoltaic/thermal (PV/T) air heating collectors: steady-state simulation. Renewable Energy 1997; 11(3): 363-385.

[9] Garg H, Adhikari RS. System performance studies on a photovoltaic/thermal (PV/T) air heating collector. Renewable Energy 1999; 16(1-4): 725-730.

[10] Bosanac M. PV/T solar collectors and their potential in Denmark. 2018.

[11] Tiwari A, Sodha MS. Parametric study of various configurations of hybrid PV/thermal air collector: Experimental validation of theoretical model. Solar Energy Materials and Solar Cells 2007; 91(1): 17-28.

[12] Chow TT, Ji J, He W. PV/T Collector System for Domestic Application. Vol. 129. 2007.

[13] Anderson TN. Performance of a building integrated photovoltaic/thermal (BIPVT) solar collector. Solar Energy 2009; 83(4): 445-455.

[14] Ibrahim, A. Efficiencies and improvement potential of building integrated photovoltaic thermal (BIPVT) system. Energy Conversion and Management 2014; 77: 527-534.

[15] Gaur A. Numerical and experimental studies on a Building integrated Semi-transparent Photovoltaic Thermal (BiSPVT) system: Model validation with a prototype test setup. Energy Conversion and Management 2016; 129: 329-343.

[16] Aste N, Beccali M, Chiesa G. Experimental evaluation of the performance of a prototype hybrid solar photovoltaic-thermal (PV/T) air collector for the integration in sloped roof. Proceedings of EPIC 2002.

[17] Good C, Andresen I, Hestnes AG. Solar energy for net zero energy buildings A comparison between solar thermal, PV and photovoltaic–thermal (PV/T) systems. Solar Energy 2015; 122: 986-996.

[18] Sathe TM, Dhoble A. A review on recent advancements in photovoltaic thermal techniques. Renewable and Sustainable Energy Reviews 2017; 76: 645-672.

[19] Hussain F. Design development and performance evaluation of photovoltaic/thermal (PV/T) air base solar collector. Renewable and Sustainable Energy Reviews 2013; 25: 431-441.

[20] Tuncer AD. Energy-exergy and enviro-economic survey of solar air heaters with various air channel modifications. Renewable Energy 2020; 160: 67-85.

[21] Zhang X. Review of R&D progress and practical application of the solar photovoltaic/thermal (PV/T) technologies. Renewable and Sustainable Energy Reviews 2012; 16(1): 599-617.

[22] Chauhan A. Comparative enviro-economic assessment and thermal optimization of two distinctly designed and experimentally validated PV/T collectors. Journal of Thermal Analysis and Calorimetry 2021; 32: 1-17.

[23] Arslan E, Aktaş M. 4E analysis of infrared-convective dryer powered solar photovoltaic thermal collector. Solar Energy 2020; 208: 46-57.

[24] Qader BS. Numerical investigation of flow through inclined fins under the absorber plate of solar air heater. Renewable Energy 2019; 141: 468-481.

[25] Versteeg HK, Malalasekera W. An introduction to computational fluid dynamics: the finite volume method. 2007: Pearson education.

[26] Yamaç Hİ. Numerical Investigation of an Exhaust Muffler System. International Conference on Advances and Innovations in Engineering (ICAIE), 2017, TURKEY, 2017.

[27] Hazami M. Energetic and exergetic performances analysis of a PV/T (photovoltaic thermal) solar system tested and simulated under to Tunisian (North Africa) climatic conditions. Energy 2016; 107: 78-94.

[28] Release AF. 15.0, ANSYS Fluent Theory Guide. ANSYS Inc, Canonsburg, PA, USA, 2013.

[29] Fluent, Ansys fluent theory guide. ANSYS Inc., USA, 2011. 15317: 724-746.

[30] Arslan E, Aktaş M, Can ÖF. Experimental and numerical investigation of a novel photovoltaic thermal (PV/T) collector with the energy and exergy analysis. Journal of Cleaner Production 2020; 123255.

[31] Sudhakar K, Srivastava T. Energy and exergy analysis of 36 W solar photovoltaic module. International Journal of Ambient Energy 2014; 35(1): 51-57.

[32] Alzaabi AA. Electrical/thermal performance of hybrid PV/T system in Sharjah, UAE. International Journal of Smart Grid and Clean Energy 2014; 3(4): 385-389.

[33] Jahromi SN, Vadiee A,Yaghoubi M. Exergy and economic evaluation of a commercially available PV/T collector for different climates in Iran. Energy Procedia 2015; 75: 444-456.

[34] Mojumder MSS. Study of hybrid photovoltaic thermal (PV/T) solar system with modification of thin metallic sheet in the air channel. J. Energy Technol. Policy 2011; 3(5): 47-55.